Research Article | Vol. 29, No. 1 / 4 January 2021 / Optics Express 315

Optics EXPRESS

Astigmatic hybrid SU(2) vector vortex beams: towards versatile structures in longitudinally variant polarized optics

ZHAOYANG WANG,[1,2] YIJIE SHEN,[3,6] DARRYL NAIDOO,[4,5] XING FU,[1,2,7] AND ANDREW FORBES[5]

[1] *Key Laboratory of Photonic Control Technology (Tsinghua University), Ministry of Education, Beijing 100084, China*
[2] *State Key Laboratory of Precision Measurement Technology and Instruments, Department of Precision Instrument, Tsinghua University, Beijing 100084, China*
[3] *Optoelectronics Research Centre & Centre for Photonic Metamaterials, University of Southampton, Southampton SO17 1BJ, United Kingdom*
[4] *CSIR National Laser Centre, PO Box 395, Pretoria 0001, South Africa*
[5] *School of Physics, University of the Witwatersrand, Private Bag 3, Wits 2050, South Africa*
[6] *y.shen@soton.ac.uk*
[7] *fuxing@mail.tsinghua.edu.cn*

Abstract: Structured light with more controllable degrees-of-freedom (DoFs) is an exciting topic with versatile applications. In contrast to conventional vector vortex beams (VVBs) with two DoFs of orbital angular momentum (OAM) and polarization, a hybrid ray-wave structure was recently proposed [Optica **7**, 820 (2020)], which simultaneously manifests multiple DoFs such as ray trajectory, coherent state phase, trajectory combination, besides OAM and polarization. Here we further generalize this exotic structure as the astigmatic hybrid VVB by hatching a new DoF of astigmatic degree. Importantly, the transverse topology varies with propagation, e.g. a linearly distributed hybrid trajectory pattern can topologically evolve to a circularly polygonal star shape, where the number of singularity changes from zero to multiple in a single beam. The propagation-dependent evolution can be easily controlled by the astigmatic degree, including as a vector vortex state such that different astigmatic trajectories have different polarizations. We experimentally generate such beams from a simple laser with a special astigmatic conversion by combined spherical and cylindrical lenses, and the results agree well with our theoretical simulation. With our new structured light, the propagation-multiplexing multi-DoF patterns can be controlled in a single beam, which can largely extend related applications such as high-dimensional large-capacity optical communication, laser machining, and particle trapping.

1. Introduction

Structured light has attracted increasingly attention for its diverse applications in both classical and quantum optics, taking advantage of its customized distribution of intensity, phase, polarization, orbital angular momentum (OAM), and other degrees-of-freedom (DoFs) [1–3]. In particular, the emergence of vector vortex beams (VVBs) [4–6], as a vectorial combination of polarization and OAM modes, has created amazing applications with on-demand DoF control, e.g. high-speed laser machining of nano-structures [7–9], driving the microrobots [10], optical tweezers for manipulating particles [11–13], high-precision metrology [14–16], kinematic sensing [17,18], high-security encryption [19,20], large-capacity multi-channel quantum and classical communications [21–25]. Therefore, it is highly topical today to generate versatile light beams with more exotic structures and controllable DoFs. For example, VVBs can have more than two DoFs, i.e. not only polarization and OAM, but also additional spatial structure, spin angular momentum, anisotropy, coherence and time dynamics, etc [26–32].

#414674 https://doi.org/10.1364/OE.414674
Journal © 2021 Received 20 Nov 2020; revised 17 Dec 2020; accepted 17 Dec 2020; published 22 Dec 2020
Corrected: 7 January 2021

Optics EXPRESS

In contrast to conventional VVB manipulated by two DoFs, i.e. OAM mode and polarization, the SU(2) geometric beam has recently demonstrated the capability of manipulating more DoFs due to its unique structure of ray-wave duality (RWD) [33–37], which can be described by both the geometric ray trajectories and coherent wave-packet. Such a geometric beam can be directly generated from a laser cavity when the cavity geometry is precisely controlled into a frequency-degenerate state that fulfills a periodic ray trajectory in laser oscillator [36–39]. Particularly, for a SU(2) geometric beam, the corresponding periodic trajectories including a cluster of rays under SU(2) symmetry, are described by a number of DoFs such as frequency-degenerate ratio, trajectory combination and coherent-state phase [40]. After introducing OAM, in contrast to the common vortex beams with a phase-singularity, the SU(2) vortex beams harness the structure of multiple singularities, resulting into both center OAM and partial OAM [41–44]. Moreover, it was discovered that finer structures on the light of each ray orbit in the geometric trajectory can also be tailored, which hatched the multi-axis vortices structure [45]. Thus for a scalar SU(2) vortex beam, many new DoFs were already manifested by its ray trajectories and multi-OAM structures. Besides, the SU(2) vector vortex beams can further involve the polarization as a DoF. Very recently, the hybrid SU(2) structure was proposed, which can combine two geometric beams together and extend the DoFs to manipulate vectorial non-separable state of light [46]. In short, the hybrid SU(2) VVB plays as an ideal candidate to meet the requirement of the development of multi-DoF structured light.

In this paper, we propose a new kind of VVBs with astigmatic hybrid trajectory structure, which introduces a new DoF, i.e. the astigmatic degree, in hybrid SU(2) geometric beams. Previously, the transverse patterns of vortex geometric beams on various transverse planes are always similar while rotating upon propagation. Here in our new astigmatic hybrid geometric beam, we show a propagation-dependent transverse topology, e.g. it can gradually evolve from linearly distributed orbits to circular polygonal star shapes during the beam propagation, revealing the complex OAM. The propagation-dependent topology is manifested by the astigmatism controlled by combined spherical and cylindrical lenses mode converter. We also realize the vector vortex state of the astigmatic hybrid geometric beam, in which different trajectories can be tuned into different polarized states by applying anisotropic gain crystal in the off-axis pumped degenerate cavity. Importantly, in this new type of beam, the topological charges and vector singularities gradually change from non-singularity to complex structures of multiple singularities upon propagation. This exotic beam topology is extremely attractive in the cutting-edge topics of high-dimensional vortices and longitudinally variable polarization optics, predicted by scientists very recently [47], holding the promise for largely extending a myriad of fundamental physical studies and practical applications of structured lights.

2. Experimental design

The experimental design includes two parts: the front-end structured light laser cavity and the external astigmatic converter with combined spherical and cylindrical lenses. The structured light laser is controlled to generate the planar geometric state of the vector hybrid SU(2) geometric beam and the astigmatic converter is used to transfer the planar geometric beam into astigmatic geometric beam with complex OAM and propagation-dependent topological charges, as shown in Fig. 1, where planar trajectories are focused on a cylindrical lens by a spherical lens with focal length f. Then the astigmatic beam evolves from planar geometric beam to circular vortex geometric beam upon propagation after passing through the cylindrical lens.

When a laser cavity is precisely controlled into a special geometry that the ratio of transverse and longitudinal mode frequency spaces is a prescribed rational number (the frequency-degenerate state $\Omega = \omega_0/\omega_z = P/Q$, where P and Q are coprime integers, ω_0 and ω_z are transverse and longitudinal mode frequency spaces), the oscillation can fulfill a ray-like periodic trajectory forming a closed path that is ever repeating back and forth [36]. The shape of trajectories and

Optics EXPRESS

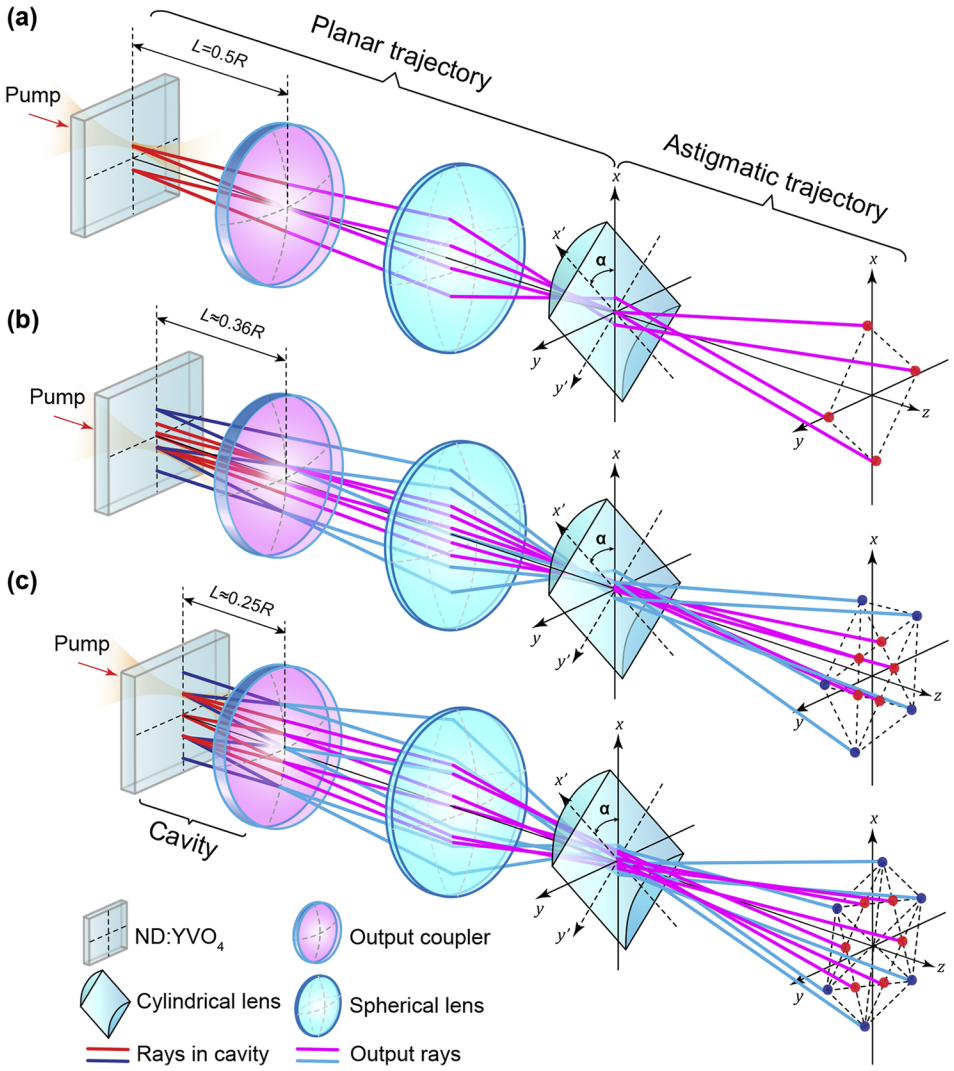

Fig. 1. Experimental design. The resonant cavity consists of a Nd:YVO_4 crystal with dichroic coating and output coupler. Planar ray oscillation would be excited by pump in cavity. R is the radius of curvature of the output coupler. α is astigmatic degree and $\alpha = \pi/4$ selected here to illustrate the experimental design. Output planar ray trajectories are focused on cylindrical lens by a spherical lens and then evolve into circularly polygonal star shape gradually in propagation. The cases for (a) $Q = 4$ without hybrid structure; (b) $Q = 5$ with hybrid structure; and (c) $Q = 6$ with hybrid structure, respectively. Pink and light blue lines represent the clusters of ray trajectories for inner sub-beam with $(\eta N_x, \eta N_y)$ $(\eta = \cos^2(2\pi/Q)/\cos^2(\pi/Q))$ and outer sub-beam with (N_x, N_y) outside cavity, respectively. Red and navy blue lines represent the inner and outer clusters of ray trajectories in cavity, respectively.

Optics EXPRESS

period of bounces are determined by the cavity length, cavity mirror curvatures, and the position of the pump light. Thus in this case, the lasing beams have a preference to be localized on the periodic ray trajectories [36]. We can use the off-axis pumping to generate the various geometric beams coupled with the periodic trajectories [37]. Although ray-like, various rays are coherent beams exhibiting a wave-like behaviour and the whole wave-packet can be described by the formalism of SU(2) coherent states [48], illustrating the salient property of RWD [49,50]. Recently, it was already reported that two geometric beams can be generated together in a single cavity as hybrid state [46], where the two trajectories have an overlapped location of inflection points sharing the pumping spot (shown in Fig. 1(b),(c) for the two examples at $|\Omega = 1/5\rangle$ and $|\Omega = 1/6\rangle$ states).

In our experiment of the geometric beam laser, a $\lambda = 808$ nm fiber-coupled laser diode (LD) (FOCUSLIGHT, FL-FCSE08-7-808-200) was used as the pump source. With a telescope system with magnification of about 1:1 constituted by two identical anti-reflective (AR) coated lenses (focal length $F = 25$ mm), the pump light was focused into a c-cut Nd:YVO_4 slice-like crystal with dopant of 0.5 at.% and thickness of 5 mm, which was wrapped in a copper heat sink and conductively water cooled at 18°C. The outside surface of crystal was AR coated at 808 nm and high-reflective coated at 1064nm and the inner surface AR coated at $\lambda = 1064$ nm. A plane-concave mirror was used as the output coupler with the radius of curvature of 100 mm, while the transmittance is 10% at 1064 nm for inner surface and AR coated for outer surface.

In contrast to the conventional astigmatic mode converter with two identical cylindrical lenses that converts a HG mode into a LG mode carrying OAM [51–54], a form of astigmatic transformation with combined spherical and cylindrical lenses has been proposed to convert more general structured light with topological phase [55,56]. The output beam from the cavity was focused by the spherical lenses to make the Rayleigh range z_R equal to f and form a new waist at a distance f in front of the cylindrical lenses [57]. The evolution of transmitted light is related to the angle α between the output beam (in x-y coordinate) and the cylindrical lens (in x'-y' coordinate) as shown in Fig. 1. In the following we will construct an analytic model to interpret this astigmatic hybrid geometric beam from the perspective of ray trajectories including the effect of α on longitudinally mode evolution and principle of vector astigmatic hybrid geometric beam generation, further to tailor a novel vector astigmatic hybrid SU(2) geometric beam with more controllable DoFs. Besides, it is worth noting that astigmatic optics are used not only as mode converters, but also for detecting the topological charge of the OAM [58,59] and also for visualization of the polarization state of VVBs [60].

3. Theoretical model

SU(2) coherent state, a quantum state with classical-resembling property, can be decomposed into a superposition of eigenstate $|K, M\rangle$ by SU(2) Lie algebra, as $|\phi\rangle = \frac{1}{2^{M/2}} \sum_{K=0}^{M} \binom{M}{K}^{1/2} e^{iK\phi} |K, M\rangle$, where K and $(M - K)$ are number of bosons in the first and second modes of eigenstate $|K, M\rangle$, M is total number of bosons and ϕ is the coherent state phase [61]. The corresponding classical analogy, SU(2) geometric beam with RWD, can be constructed just by replacing state $|K, M\rangle$ with a set of frequency-degenerate eigenmode as $\Phi = \frac{1}{2^{M/2}} \sum_{K=0}^{M} \binom{M}{K}^{1/2} e^{iK\phi} \psi_{n+pK,m+qK,l+sK}$, where $\psi_{n+pK,m+qK,l+sK}$ is frequency-degenerate eigenmode with $p + q = Q$ and $s = -P$ [36]. The wave-packet of SU(2) geometric beam is coupled with classical trajectories, thus so-called SU(2) geometric beam [35–39]. In this section, we would research the classical trajectories and the corresponding wave-packet of hybrid SU(2) geometric beam, a superposition of two SU(2) geometric beams with specific geometric relations firstly. Then a novel astigmatic hybrid SU(2)

Optics EXPRESS

geometric beam with longitudinally variant topology is constructed by hatching a new DoF of astigmatic degree α, which would evolve from hybrid planar geometric beam to hybrid vortex (star-shaped) geometric beam in propagation for $\alpha = \pi/4$. Besides, we would tailor a novel longitudinally variant vector structured light, vector astigmatic hybrid SU(2) geometric beam, by coupling various polarizations in two decomposed astigmatic SU(2) geometric beams.

3.1. Hybrid SU(2) geometric beam with ray-wave structure

Without loss of generality, we consider a stable plano-concave cavity consisting of a concave mirror with radius of curvature R and a planar mirror for discussions. The structure of laser beams mainly depends on the ratio P/Q. Without astigmatism, when the effective cavity length L fullfills $L = z_R \tan(\pi P/Q)$ where z_R is Rayleigh range, the classical trajectories for SU(2) geometric beam in frequency-degenerate cavity can be derived as [48,62]:

$$\begin{cases} x_s(z) = \sqrt{N_x} w(z) \cos[\theta_s + \phi_x \pm \theta_G(z)] \\ y_s(z) = \sqrt{N_y} w(z) \cos[\theta_s + \phi_y \pm \theta_G(z)] \end{cases}, \tag{1}$$

where $\theta_s = (2\pi s)(P/Q)$, $s = 0, 1, 2, \ldots, Q-1$ is running index of periodic geometric trajectories, ϕ_x and ϕ_y are phase factors related to coherent state phase ϕ, transverse indices N_x and N_y determining transverse scale in x- and y- directions, $\theta_G(z)$ Gouy phase, $w(z) = w_0\sqrt{1 + (z/z_R)}$ Gaussian beam waist parameter, $z_R = w_0^2\pi/\lambda$ the Rayleigh range, λ the wavelength, + and − represent the ray trajectories of forward and backward propagation, respectively.

Then we could obtain the wave-packet of hybrid SU(2) geometric beam from classical trajectories Eq. (1) as [62]:

$$\Phi(\tilde{x}, \tilde{y}, \tilde{z}) = \sum_{s=0}^{Q-1} \varphi_s(\tilde{x}, \tilde{y}, \tilde{z}), \tag{2}$$

$$\varphi_s(\tilde{x}, \tilde{y}, \tilde{z}) = \frac{1}{Q} G(\tilde{x}, \tilde{y}, \tilde{z}) F(\tilde{x}, u_s^{\pm}) F(\tilde{y}, v_s^{\pm}) \mathrm{e}^{\mathrm{i}(N_x+N_y)(2\pi s)P/Q}, \tag{3}$$

where $G(\tilde{x}, \tilde{y}, \tilde{z}) = \pi^{-1/2}\mathrm{e}^{-(\tilde{x}^2+\tilde{y}^2)(1+\mathrm{i}\tilde{z})/2}\mathrm{e}^{\mathrm{i}(N_x+N_y)\theta_G(z)}$, $F(\tilde{x}, u_s^{\pm}) = \mathrm{e}^{-[(u_s^{\pm})^2+|u_s^{\pm}|^2-2\sqrt{2}u_s^{\pm}\tilde{x}]/2}$, $F(\tilde{y}, v_s^{\pm}) = \mathrm{e}^{-[(v_s^{\pm})^2+|v_s^{\pm}|^2-2\sqrt{2}v_s^{\pm}\tilde{y}]/2}$, $\tilde{x} = \sqrt{2}x/w(z) = \sqrt{2}\mathrm{Re}(u_s^{\pm})$, $\tilde{y} = \sqrt{2}y/w(z) = \sqrt{2}\mathrm{Re}(v_s^{\pm})$, $\tilde{z} = z/z_\mathrm{R}$, $u_s^{\pm}(z) = \sqrt{N_x}\mathrm{e}^{-\mathrm{i}[\theta_s+\phi_x\pm\theta_G(z)]}$, $v_s^{\pm}(z) = \sqrt{N_y}\mathrm{e}^{-\mathrm{i}[\theta_s+\phi_y\pm\theta_G(z)]}$. $\varphi_s(\tilde{x}, \tilde{y}, \tilde{z})$ reveals that each classical trajectory labeled s corresponds to a Gaussian wave packet. And it was demonstrated that $\Phi(\tilde{x}, \tilde{y}, \tilde{z})$ is equivalent to SU(2) geometric beam in Supplement of [46], where the parameters' relations between $(N_x, N_y, \phi_x, \phi_y)$ and (n, m, ϕ) are as $N_x \propto n$, $N_y \propto m$ [63], $\phi_x = \phi/Q$ [46], ϕ_y is not considered for planar state since $N_y = 0$ while OAM state requires $|\phi_x - \phi_y| = \pi/2$ for forming the spatial ray trajectory [62]. Since the structure of SU(2) geometric beam is determined by transverse indices (N_x, N_y) and coherent state phase ϕ, the corresponding cluster of classical trajectories can be noted as $\{(x_s, y_s, z)\}_{N_x,N_y,\phi}$.

Classical trajectory offers us an intuitive tool to construct and tailor novel structured light [46,64]. Recently a novel hybrid structured light has been proposed [46], a hybrid superposition of two SU(2) vortex geometric beams with specific geometric relations: $|\phi_i - \phi_j| = \pi/Q$ and $N_i/N_j = \cos^2(2\pi/Q)/\cos^2(\pi/Q)$ $(i, j = 1, 2)$, where subscripts i, j correspond to two decomposed beams of hybrid SU(2) geometric beam, respectively. The two decomposed beams can be resonated in cavity with off-axis pumping simultaneously and form a star-shaped beam with exotic vortex structure. The specific geometric relations reveal that the relation of the transverse indices of two decomposed beams is linear as $(N_x, N_y)_i = \eta(N_x, N_y)_j$, $\eta = \cos^2(2\pi/Q)/\cos^2(\pi/Q)$. Thus the corresponding cluster of hybrid classical trajectories noted as $\{(x_s, y_s, z)\}_\mathrm{h}$ can be expressed

Optics EXPRESS

as

$$\{(x_s, y_s, z)\}_{\mathrm{h}} = \{(x_s, y_s, z)\}_{N_x,N_y,\phi} + \{(x_s, y_s, z)\}_{\eta N_x,\eta N_y,\phi+\pi}\,, \tag{4}$$

where Q>4, since hybrid SU(2) geometric beam with $Q \leq 4$ can not be resonated in cavity simultaneously [46]. The decomposed beam with larger transverse indices has a larger scale thus called outer sub-beam and the other one the inner sub-beam. Due to η<1 for Q>4, thus $\{(x_s, y_s, z)\}_{\eta N_x,\eta N_y,\phi+\pi}$ corresponds to the cluster of classical trajectories of inner sub-beam and $\{(x_s, y_s, z)\}_{N_x,N_y,\phi}$ corresponds to the cluster of trajectories of outer sub-beam, respectively.

The wave-packet of outer sub-beam can be obtained by substituting the classical trajectories $\{(x_s, y_s, z)\}_{N_x,N_y,\phi}$ into Eq. (2). Analogously, substituting the classical trajectories $\{(x_s, y_s, z)\}_{\eta N_x,\eta N_y,\phi+\pi}$ into Eq. (2) would lead to the wave-packet of inner sub-beam. Since hybrid SU(2) geometric beam is the superposition of two decomposed beams with specific geometric relations fundamentally, the wave-packet of hybrid SU(2) geometric beam can be obtained by substituting the classical trajectories $\{(x_s, y_s, z)\}_{\mathrm{h}}$ into Eq. (2) as:

$$\Phi_{\mathrm{h}}(\tilde{x}, \tilde{y}, \tilde{z}) = \Phi_{N_x,N_y,\phi}(\tilde{x}, \tilde{y}, \tilde{z}) + \Phi_{\eta N_x,\eta N_y,\phi+\pi}(\tilde{x}, \tilde{y}, \tilde{z}), \tag{5}$$

where $\Phi_{N_x,N_y,\phi}(\tilde{x}, \tilde{y}, \tilde{z})$ and $\Phi_{\eta N_x,\eta N_y,\phi+\pi}(\tilde{x}, \tilde{y}, \tilde{z})$ are wave-packets of outer and inner sub-beams, respectively.

3.2. Astigmatic hybrid SU(2) geometric beam

Astigmatism was reported only in SU(2) geometric beam [45,57] and has never been researched in hybrid SU(2) geometric beam. Hereinafter, we will derive a set of mathematical formulas for characterizing the topological evolution of astigmatic hybrid SU(2) geometric beam in the perspective of classical trajectories providing a physical insight in the picture of semi-classical RWD [49,50]. Selecting $z = 0$ as the position of the cylindrical lens, the cylindrical lenses can make a difference for Gouy phase in $x'-$ and $y'-$ axis labeled in Fig. 1 as $\theta_{G,x'}(z) = \pi/2 + \tan^{-1}(\frac{z-z_R}{z_R})$, $\theta_{G,y'}(z) = \tan^{-1}(\frac{z+z_R}{z_R})$ [52,57]. In addition, Gaussian beam waist parameter in $x'-$ and $y'-$ axis need to be modified as $w_{x'}(z) = w_0\sqrt{1 + (\frac{z-z_R}{z_R})^2}$, $w_{y'}(z) = w_0\sqrt{1 + (\frac{z+z_R}{z_R})^2}$ [57]. Since the trajectories of output beam from cavity is located on a plane generally as shown in Fig. 1, the parameters (N_x, N_y) for which can be selected as $(N, 0)$. To facilitate the analysis of astigmatism, a transformation of coordinates from (x, y) to (x', y') is required to perform beforehand as:

$$\begin{bmatrix} x'_s \\ y'_s \end{bmatrix} = R(\alpha)\begin{bmatrix} x_s \\ 0 \end{bmatrix} = \begin{bmatrix} \cos(\alpha) & \sin(\alpha) \\ -\sin(\alpha) & \cos(\alpha) \end{bmatrix}\begin{bmatrix} x_s \\ 0 \end{bmatrix}, \tag{6}$$

where α is the rotating angle between (x, y) and (x', y'), as shown in Fig. 1. Thus the astigmatic classical trajectories in (x', y') coordinate can be explicitly derived as:

$$\begin{cases} x'_s(z) = \sqrt{N}\cos(\alpha)w_{x'}(z)\cos[\theta_s + \phi_x \pm \theta_{G,x'}(z)] \\ y'_s(z) = -\sqrt{N}\sin(\alpha)w_{y'}(z)\cos[\theta_s + \phi_x \pm \theta_{G,y'}(z)] \end{cases}, \tag{7}$$

The mathematical expressions of astigmatic geometric beam have been derived since corresponding expression in (x, y) coordinate requires only an inverse transformation as $(x_s^{\mathrm{A}}, y_s^{\mathrm{A}})^{\mathrm{T}} = R(-\alpha)(x'_s, x'_s)$, where superscript 'A' is used to distinguish from non-astigmatic classical trajectories in Eq. (4) and superscript 'T' represents matrix transpose. Then we can obtain the wave packet of astigmatic beams by substituting the astigmatic classical trajectories (x'_s, y'_s, z) into Eq. (2) as $\Phi(x'_s, y'_s, z)$ $(x_s \to x'_s, y_s \to y'_s)$, which is equivalent to the wave-packet of astigmatic SU(2) geometric beam as $\Phi = \frac{1}{2^{M/2}}\sum_{K=0}^{M}\binom{M}{K}^{1/2} \mathrm{e}^{\mathrm{i}K\phi}\psi'_{n+pK,m+qK,l+sK}$ in which the eigenmodes are just replaced by astigmatic eigenmodes $(\psi \to \psi')$ [45,57].

Optics EXPRESS

Since the cluster of classical trajectories of astigmatic hybrid SU(2) geometric beam is equal to a superposition of classical trajectories of inner and outer astigmatic beams, we can further get the mathematical formulas of classical trajectories of astigmatic hybrid SU(2) geometric beam as $\{(x_s', y_s', z)\}_{\mathrm{h}} = \{(x_s', y_s', z)\}_{N_x,N_y,\phi} + \{(x_s', y_s', z)\}_{\eta N_x,\eta N_y,\phi+\pi}$ by substituting Eq. (7) to Eq. (4). Then the corresponding wave-packet of astigmatic hybrid SU(2) geometric beam can be derived as $\Phi_{\mathrm{h}}(x_s', y_s', z) = \Phi_{N_x,N_y,\phi}(x_s', y_s', z) + \Phi_{\eta N_x,\eta N_y,\phi+\pi}(x_s', y_s', z)$ based on Eq. (5), where $\Phi_{N_x,N_y,\phi}(x_s', y_s', z)$ is wave-packet of astigmatic outer sub-beam and the other one the inner sub-beam, respectively.

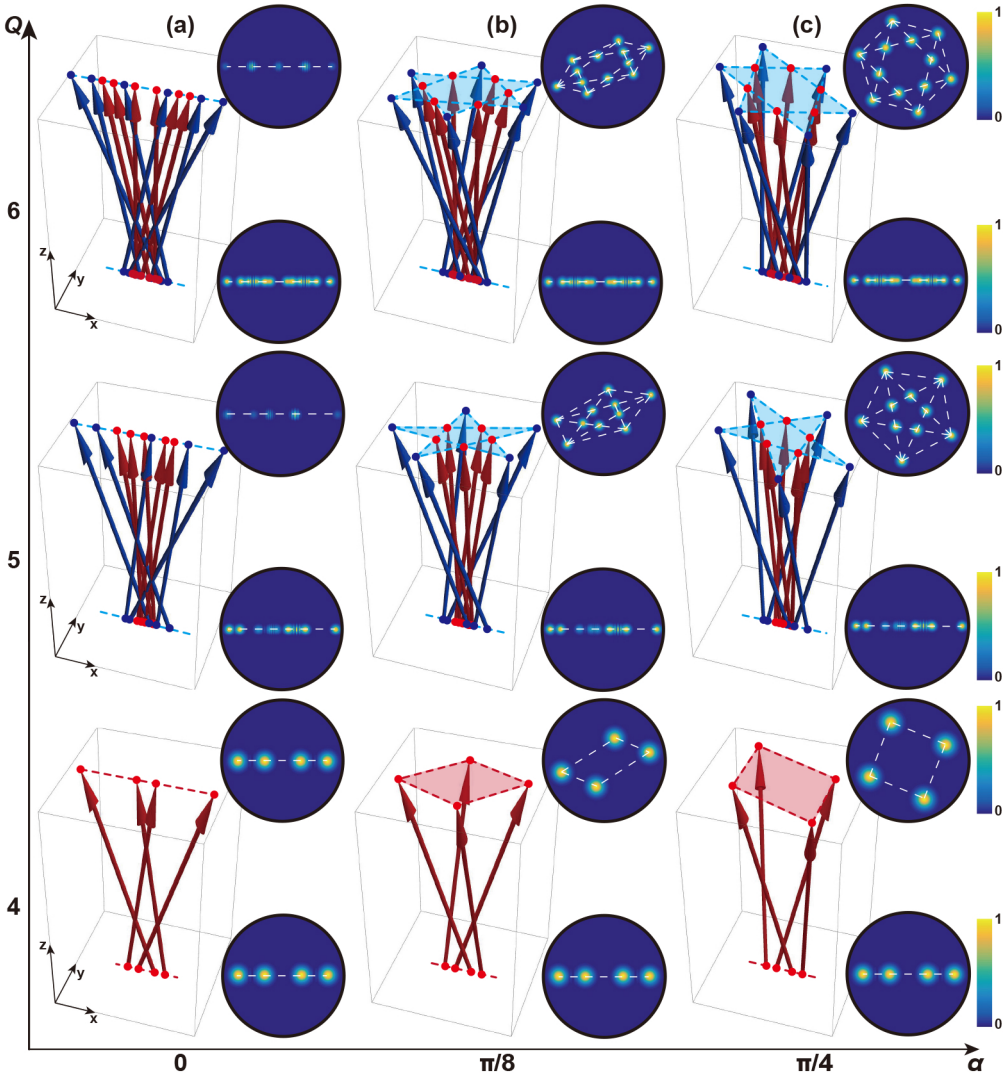

Fig. 2. Classical trajectories with corresponding transverse modes for astigmatic hybrid SU(2) geometric beam. The range z of classical trajectories is $0 - 5z_R$. The transverse modes on top and bottom of subplots are intensity distributions at $z = 100z_R$ and 0, respectively. (a) $\alpha = 0$ non-astigmatism essentially; (b) $\alpha = \pi/8$; (c) $\alpha = \pi/4$. The cases for $Q = 4$ without hybrid structure and $Q = 5, 6$ with hybrid structure. Red and blue lines represent the clusters of classical trajectories for inner and outer sub-beams, respectively. (Colormap: darkness to brightness means 0 to 1 for intensity.)

Optics EXPRESS

The classical trajectories and intensity distributions in (x, y) coordinate of astigmatic (hybrid) SU(2) geometric beam are shown in Fig. 2 for $(P, Q) = (1, 4), (1, 5)$ and $(1, 6)$ respectively. In order to provide a clear view of near field, the classical trajectories sketched in Fig. 2 only cover the range $0 - 5z_R$ before it expands too large in propagation. The transverse modes in the near field ($z = 0$) and far field ($z = 100z_R$) are attached in each subplot of Fig. 2. When $\alpha = 0$, classical trajectories are still located on a plane without astigmatism. When $\alpha = \pi/8$, astigmatic SU(2) geometric beam evolves from planar to elliptical multi-path beam in propagation with longitudinally variant characteristics. When $\alpha = \pi/4$, astigmatic planar geometric beam will evolve to vortex multi-path beam at far field ($z = 100z_R$). The parameter α modulates the mode evolution longitudinally and provides a new DoF for structured light, having the potential to offer an useful tool for longitudinally variant polarized optics. In addition, the classical trajectories for $(P, Q) = (1, 5)$ and $(1, 6)$ can be decomposed into two groups of astigmatic classical trajectories, one with smaller transverse indices $(\eta N_x, \eta N_y)$ for red trajectories and another with larger transverse indices (N_x, N_y) for blue trajectories, as shown in Fig. 3. And these two decomposed astigmatic SU(2) geometric beams with specific geometric relations can be resonated in cavity and modulated out simultaneously [46]. The principles about the generation of astigmatic hybrid SU(2) geometric beam are shown in Fig. 3, where the red (inner) and blue (outer) trajectories represent a smaller scale beam and larger one respectively. When $\alpha = \pi/4$, the astigmatic classical trajectories of planar SU(2) geometric beam (at $z = 0$) would diverge to form a star-shaped distribution (at far field). Besides, the phase distribution of scalar astigmatic

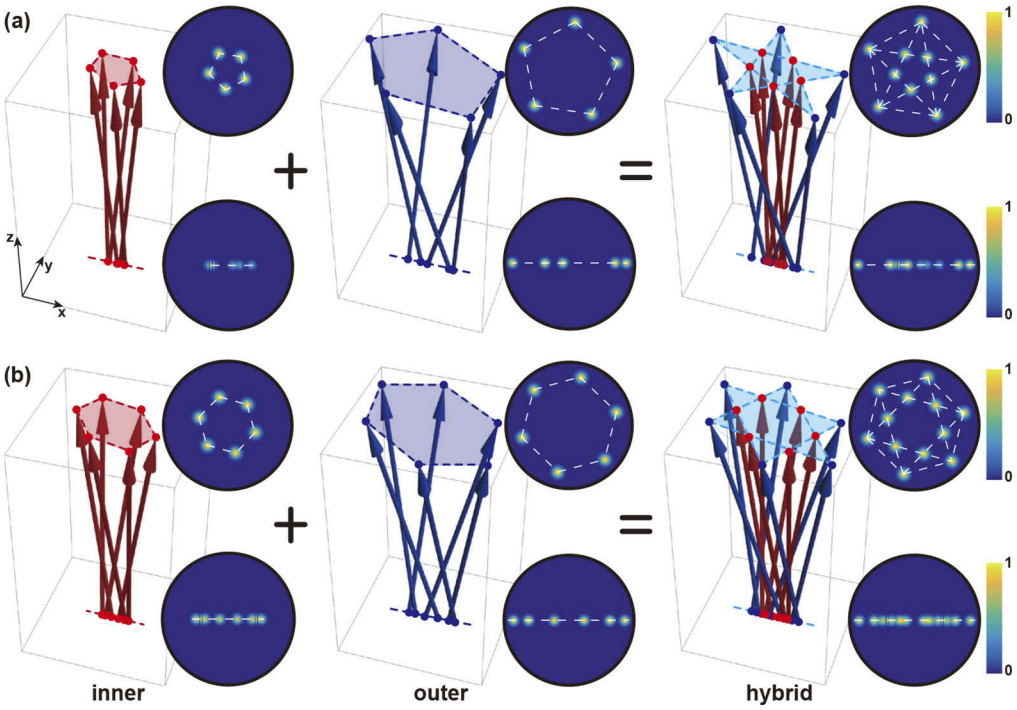

Fig. 3. Generation principles for astigmatic hybrid SU(2) geometric beam. The transverse modes on top and bottom rows are intensity distributions at $z = 100z_R$ and 0 in subplots, respectively. The range z of classical trajectories is $0 - 5z_R$ and $\alpha = \pi/4$ selected here. (a) $Q = 5$; (b) $Q = 6$. Red and blue lines represent the clusters of ray trajectories for inner and outer sub-beams, respectively. (Colormap: darkness to brightness means 0 to 1 for intensity.)

Optics EXPRESS

hybrid geometric beam performs longitudinally variant singularity in propagation as shown in Fig. 4. And a novel vector structured light with longitudinally variant polarization singularity is constructed based on astigmatic hybrid SU(2) geometric beam in next subsection.

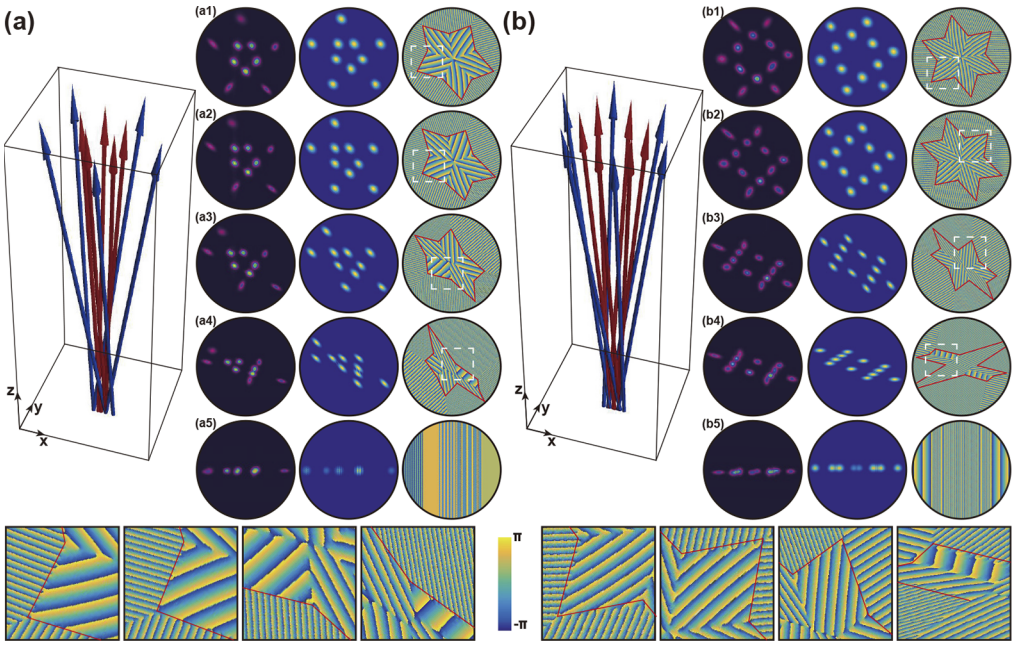

Fig. 4. Scalar astigmatic hybrid SU(2) geometric beam with longitudinally variant phase singularities. (a) $|\Omega = 1/5\rangle$; (b) $|\Omega = 1/6\rangle$. The left column is the classical trajectories of astigmatic hybrid SU(2) geometric beam in the range of z from 0 to $5z_R$ and $\alpha = \pi/4$ selected. Red and blue lines represent the clusters of classical trajectories for inner and outer sub-beams, respectively. The first, second and third columns are experimental results, theoretical intensity and phase distributions at some transverse planes. The red line is the boundary of the regions between severe and moderate phase variation. The subplots on bottom row are partial enlarged details for phase distributions in white square labeled in (a1)-(a4) and (b1)-(b4), respectively. (Colormap: darkness to brightness means 0 to 1 for intensity and $-\pi$ to π for phase.)

3.3. *Vector astigmatic hybrid SU(2) geometric beam*

In addition to longitudinally variant phase singularity, astigmatic hybrid SU(2) geometric beam also offers us a potential way to construct an exotic longitudinally variant polarized structured light by coupling various polarizations in inner and outer sub-beams, as an example:

$$|\Phi_h\rangle = \Phi_{N_x,N_y,\phi}(x_s', y_s', z)|H\rangle + \Phi_{\eta N_x,\eta N_y,\phi+\pi}(x_s', y_s', z)|V\rangle, \tag{8}$$

where $|H\rangle$ and $|V\rangle$ represent horizontal and vertical polarizations, respectively. Besides, the coupled polarizations could be generalized to other states such as circular and vertical polarizations as shown in Fig. 5(a). Vector astigmatic hybrid SU(2) geometric beam has exotic longitudinally variant singularities and topological phase, the polarization of which depends on propagation parameter z. Two parameters, $\Theta_1 = \tan^{-1}(|E_x|/|E_y|)$ and $\Theta_2 = \tan^{-1}(E_x/E_y)$, are defined to characterize the vector property of structured light [46], where E_x and E_y are the horizontal and vertical components of structured light, respectively. The parameter Θ_1 (varying from 0 to $\pi/2$) reveals the relative distribution of intensity of polarized component

Optics EXPRESS

that $\Theta_1 = 0, \pi/4, \pi/2$ correspond to horizontal, circular and vertical polarization states. The parameter Θ_2 depicts the distribution of polarization singularities of the vector structured light and would be reduced into phase for scalar field. The novel longitudinally variant polarization property would extend structured light in applications such as optical tweezers and exploration of manipulating technologies [47]. The experimental results and detailed discussion about longitudinally variant structured light constructed by astigmatic hybrid SU(2) geometric beam are presented in next section.

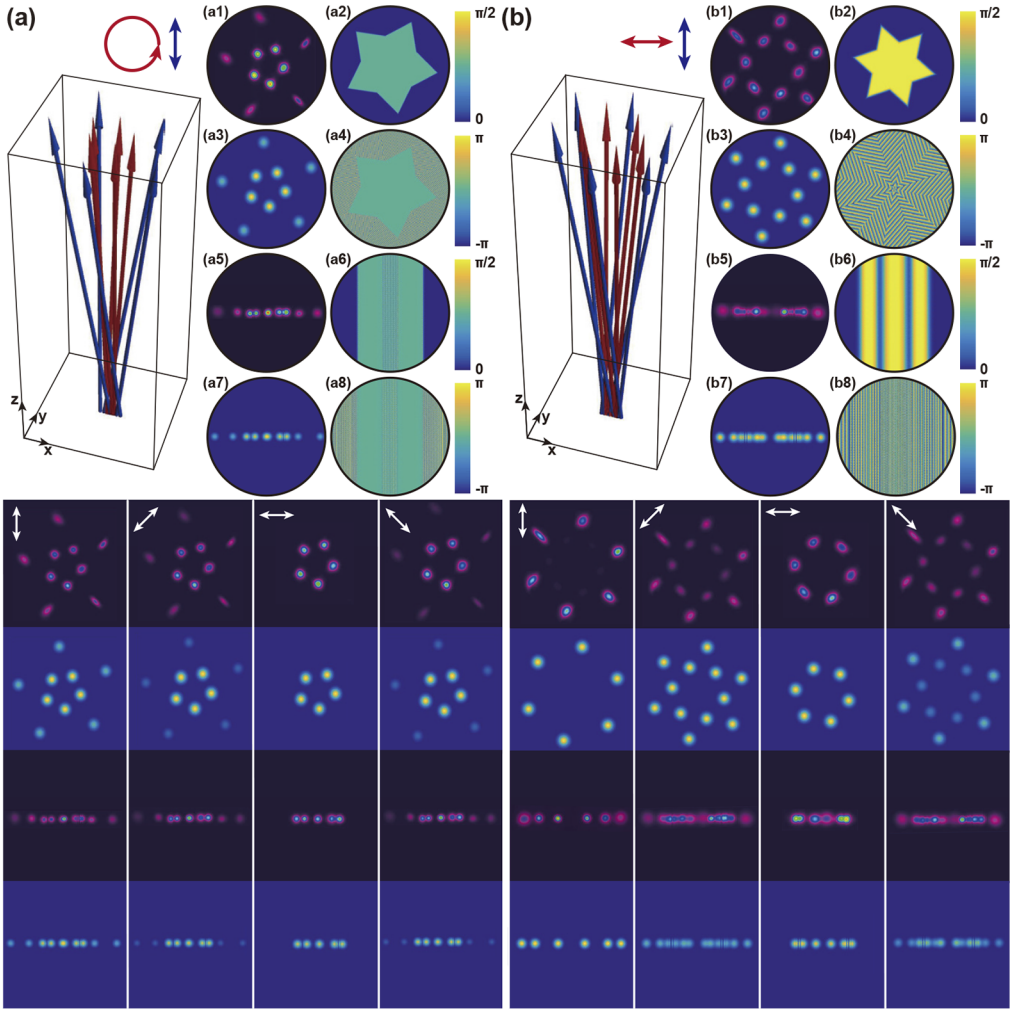

Fig. 5. Vector astigmatic hybrid SU(2) geometric beam with longitudinally variant polarization singularities. The range z of classical trajectories is $0-5z_R$ and $\alpha = \pi/4$ selected. Red and blue trajectories correspond to inner sub-beam with circular polarization and outer sub-beam with vertical polarization in (a) $|\Omega = 1/5\rangle$, and inner sub-beam with horizontal polarization and outer sub-beam with vertical polarization in (b) $|\Omega = 1/6\rangle$, respectively. The white arrows in bottom section represent orientation of the polarizer. The transverse modes are hybrid planar SU(2) geometric beams at near field and hybrid SU(2) vortex (star-shaped) geometric beams at far field. Subplots (a1),(a5),(b1),(b5) and (a3),(a7),(b3),(b7) are experimental and theoretical intensities, respectively. Subplots (a2),(a6),(b2),(b6) and (a4),(a8),(b4),(b8) are Θ_1 and Θ_2 distributions, respectively. (Colormap: darkness to brightness means 0 to 1 for intensity, 0 to $\pi/2$ for Θ_1, and $-\pi$ to π for Θ_2.)

Optics EXPRESS

4. Results

4.1. Longitudinally variant phase singularities

The experimental results present transverse distributions of astigmatic hybrid SU(2) geometric beam for $(P, Q) = (1, 5)$ and $(1, 6)$ at some planes, demonstrating the evolution from hybrid planar SU(2) geometric beam at near field to hybrid vortex (star-shaped) geometric beam at far field in Fig. 4. The corresponding theoretical intensity and phase distributions are attached in the right columns of experimental results. The length of plane-concave cavity can be calculated by $L = R\sin^2(\pi P/Q)$, where R =100 mm is the radius of curvature of output coupler [36]. Thus $L \approx$36 mm, 25 mm, for $(P, Q) = (1, 5)$ and $(1, 6)$, respectively. Since the outer sub-beam has larger transverse indices than the inner sub-beam, the phase distribution in outer region varies more frequently than in inner region, with red line labeling the boundary between these two regions. Partial enlarged manifestations of white square in Fig. 4(a1)-(a4) and (b1)-(b4) are shown in bottom section of Fig. 4, which clearly demonstrates that leap of phase variation across the boundary. To a certain extent, the shape of red line would reveal the property of longitudinally variant phase singularity, varying from irregular polygon at near field to star-shape at far field. More intriguingly, astigmatic hybrid SU(2) geometric beam with various coupled polarizations would have exotic vector property in the following subsection.

4.2. Longitudinally variant polarization singularities

We generate and study the property of longitudinally variant singularities and topological phase of two vector astigmatic hybrid SU(2) geometric beams as examples shown in Fig. 5. The red and blue symbols represent circular and vertical polarizations in Fig. 5(a), and horizontally and vertical polarizations in Fig. 5(b). The white symbols represent the orientation of polarizer. The experimental and theoretical transverse distributions are hybrid vortex (star-shaped) beams at far field and hybrid planar beams at near field, respectively.

For the beam $|\Phi_{\mathrm{h}}\rangle = \Phi_{N_x,N_y,\phi}(x_s', y_s', z)|L\rangle + \Phi_{\eta N_x,\eta N_y,\phi+\pi}(x_s', y_s', z)|V\rangle$ [Fig. 5(a)], the light field localized on the inner trajectories is circularly polarized, and thus its intensity is independent of orientation of polarizer; while the outer sub-beam is vertically linearly polarized, and thus its intensity would vanish through the polarizer with horizontal orientation, and reach the maximum with vertical orientation as shown in bottom section of Fig. 5(a). For the beam $|\Phi_{\mathrm{h}}\rangle = \Phi_{N_x,N_y,\phi}(x_s', y_s', z)|H\rangle + \Phi_{\eta N_x,\eta N_y,\phi+\pi}(x_s', y_s', z)|V\rangle$ [Fig. 5(b)], the light fields localized on the inner and outer trajectories are orthogonally polarized. Thus the vector beam would be reduced into a scalar astigmatic SU(2) geometric beam through a vertically or horizontally oriented polarizer as shown in bottom section of Fig. 5(b). Figure 5(a2) and (b2) show the distributions of Θ_1 at far field clearly demonstrating the critical region of chaotic polarized states along a star-shaped line. Distributions of Θ_1 at near field are stripes as shown in Fig. 5(a6) and (b6). The distributions of Θ_2 manifest more refined topological information about vector structured light, as shown in Fig. 5(a4),(a8),(b4),(b8). For vector beam $|\Phi_{\mathrm{h}}\rangle$ shown in Fig. 5(a) at far field, almost all the polarization singularities are located on the outer sub-beam region, as shown in Fig. 5(a4), since $E_{\mathrm{x}}/E_{\mathrm{y}}$ is a constant for light with circular polarization. For vector beam $|\Phi_{\mathrm{h}}\rangle$ shown in Fig. 5(b) at far field, consisting of inner and outer sub-beams with orthogonal polarizations, the polarization singularities are distributed over the entire field, as shown in Fig. 5(b4).

5. Discussion

Furthermore, astigmatic hybrid SU(2) geometric beam defined by $\Phi_{\mathrm{h}}(x_s', y_s', z)$ can be decomposed into a set of sub-beams $\varphi_s(x_s', y_s', z)$ located on each classical trajectory, which has the potential to tailor vector structured light with much more DoFs by manipulating each sub-beam $\varphi_s(x_s', y_s', z)$. Modulating the polarization of beams attached to each classical trajectory of astigmatic hybrid

Optics EXPRESS

SU(2) geometric beam can generate a novel longitudinally variant vector beams as shown in Fig. 6. Such vector structured light has more general controllable DoFs [40]. A generalized vector astigmatic hybrid SU(2) geometric beam can be expressed as:

$$|\Phi_{\mathrm{h}}\rangle = (\sum_{s=0}^{Q-1} \varphi_s(x'_s, y'_s, z)|\sigma_{1,s}\rangle)_{N_x,N_y,\phi} + (\sum_{s=0}^{Q-1} \varphi_s(x'_s, y'_s, z)|\sigma_{2,s}\rangle)_{\eta N_x,\eta N_y,\phi+\pi}, \tag{9}$$

where $|\sigma_{i,s}\rangle$ $(i = 1, 2,\ s = 0, 1, \ldots, Q-1)$ represents polarization of beams located on each trajectory of astigmatic hybrid SU(2) geometric beam, respectively. For example, consider two polarization states only and assume that there are only two values of $\sigma_{i,s}$, where $\sigma_{i,s} = -1, 1$ represents left-handed circle, and right-handed circular polarizations, respectively. Thus the vector astigmatic hybrid SU(2) geometric beam would have 2^{2Q} vector states with longitudinally variant singularities and topological phase. For a general case that there are n polarization states, the vector astigmatic hybrid SU(2) geometric beam would have n^{2Q} vector states. In addition, the various polarizations coupled in each sub-beam are shown in Fig. 6. The white

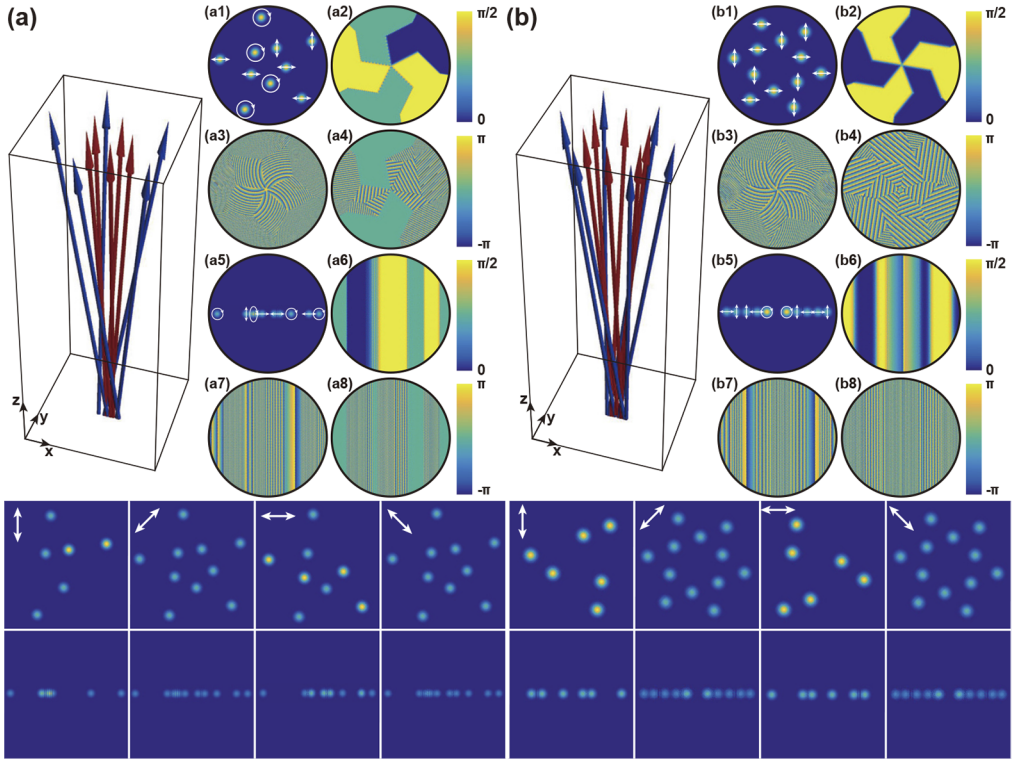

Fig. 6. Vector astigmatic hybrid SU(2) geometric beam with complex coupled polarizations. The range z of classical trajectories is $0 - 5z_R$. Red and blue trajectories correspond to inner and outer sub-beams. $\alpha = \pi/4$ selected. (a) $|\Omega = 1/5\rangle$; (b) $|\Omega = 1/6\rangle$. The white arrows in subplots (a1),(a5),(b1),(b5) represent polarizations coupled in each sub-beam. The white arrows in bottom section represent orientation of the polarizer. The transverse modes are hybrid planar SU(2) geometric beams at near field and hybrid vortex (star-shaped) SU(2) geometric beams at far field. Subplots (a1),(a5),(b1),(b5) and (a3),(a7),(b3),(b7) are theoretical intensity and phase distributions, respectively. Subplots (a2),(a6),(b2),(b6) and (a4),(a8),(b4),(b8) are Θ_1 and Θ_2 distributions, respectively. (Colormap: darkness to brightness means 0 to 1 for intensity, $-\pi$ to π for phase, 0 to $\pi/2$ for Θ_1, and $-\pi$ to π for Θ_2.)

Optics EXPRESS

arrows in Fig. 6(a1)(a5)(b1)(b5) represent various polarizations coupled in sub-beams, leading to flower-shape distributions with five (Fig. 6(a2)) and six (Fig. 6(b2)) petals of Θ_1, respectively. Polarizations coupled in each sub-beam of astigmatic hybrid SU(2) geometric beam is feasible and significant to inspire more controllable DoFs [40]. The vector astigmatic hybrid SU(2) geometric beams have almost unlimited potential in tailoring structured light with more controllable DoFs in theory. Here we have realized the hybrid ray-wave beams at frequency-degenerate states of $|\Omega = 1/5\rangle$ and $|\Omega = 1/6\rangle$. Notably, we expect to realize more complex fractional frequency-degenerate states of general $|\Omega = P/Q\rangle$ to extend more controllable DoFs by improving the precision of devices in the future work, which is of significance to further exploring the related applications in longitudinally variant polarized optics, optical manipulation and communication, etc.

6. Conclusion

In conclusion, we construct a novel type of structured light with an exotic ray-wave structure, astigmatic hybrid SU(2) VVBs, by hatching an additional DoF of astigmatic degree α in multi-DoF hybrid SU(2) geometric beam from the perspective of classical ray trajectories. The astigmatic degree is presented to manifest seminal topology of complex OAM and polarization in hybrid ray-wave structure. In contrast to conventional beam, our new structured light beam has longitudinally-variant spatial twisted ray-wave structure and vector singularities upon propagation, which can inspire explorations in the cutting-edge topics of high-dimensional vortices and longitudinally variable polarization optics. We also design a convenient and compact device for tailoring such high-dimensional vectorial structured light and generate various experimental results in degenerate states $|\Omega = 1/5\rangle$ and $|\Omega = 1/6\rangle$, demonstrating the longitudinally variant topology and singularities that well agree with our theoretical simulation. Furthermore, we illustrate that astigmatic hybrid SU(2) VVBs unveil more controllable DoFs than any other prior beams that are convenient for extending new applications for higher-dimensional optical communication, laser machining, particle trapping and manipulation.

Funding. National Key Research and Development Program of China (2017YFB1104500); Marie S.-Curie MULTIPLY Fellowship (GA713694); Beijing Young Talents Support Project (2017000020124G044); National Natural Science Foundation of China (61975087).

Disclosures. The authors declare no conflicts of interest.

References

1. A. Forbes, "Structured light from lasers," Laser Photonics Rev. **13**(11), 1900140 (2019).
2. H. Rubinsztein-Dunlop, A. Forbes, M. V. Berry, M. R. Dennis, D. L. Andrews, M. Mansuripur, C. Denz, C. Alpmann, P. Banzer, and T. Bauer, "Roadmap on structured light," J. Opt. **19**(1), 013001 (2017).
3. Y. Shen, X. Wang, Z. Xie, C. Min, X. Fu, Q. Liu, M. Gong, and X. Yuan, "Optical vortices 30 years on: OAM manipulation from topological charge to multiple singularities," Light: Sci. Appl. **8**(1), 90 (2019).
4. C. Rosales-Guzmán, B. Ndagano, and A. Forbes, "A review of complex vector light fields and their applications," J. Opt. **20**(12), 123001 (2018).
5. Z. Liu, Y. Liu, Y. Ke, Y. Liu, W. Shu, H. Luo, and S. Wen, "Generation of arbitrary vector vortex beams on hybrid-order Poincaré sphere," Photonics Res. **5**(1), 15–21 (2017).
6. U. Levy, Y. Silberberg, and N. Davidson, "Mathematics of vectorial Gaussian beams," Adv. Opt. Photonics **11**(4), 828–891 (2019).
7. T. Omatsu, K. Miyamoto, K. Toyoda, R. Morita, Y. Arita, and K. Dholakia, "A new twist for materials science: The formation of chiral structures using the angular momentum of light," Adv. Opt. Mater. **7**(14), 1801672 (2019).
8. J. Ni, C. Wang, C. Zhang, Y. Hu, L. Yang, Z. Lao, B. Xu, J. Li, D. Wu, and J. Chu, "Three-dimensional chiral microstructures fabricated by structured optical vortices in isotropic material," Light: Sci. Appl. **6**(7), e17011 (2017).
9. K. Toyoda, F. Takahashi, S. Takizawa, Y. Tokizane, K. Miyamoto, R. Morita, and T. Omatsu, "Transfer of light helicity to nanostructures," Phys. Rev. Lett. **110**(14), 143603 (2013).
10. S. Palagi, A. G. Mark, S. Y. Reigh, K. Melde, T. Qiu, H. Zeng, C. Parmeggiani, D. Martella, A. Sanchez-Castillo, N. Kapernaum, F. Giesselmann, D. S. Wiersma, E. Lauga, and P. Fischer, "Structured light enables biomimetic swimming and versatile locomotion of photoresponsive soft microrobots," Nat. Mater. **15**(6), 647–653 (2016).
11. M. Padgett and R. Bowman, "Tweezers with a twist," Nat. Photonics **5**(6), 343–348 (2011).

Optics EXPRESS

12. M. Woerdemann, C. Alpmann, M. Esseling, and C. Denz, "Advanced optical trapping by complex beam shaping," Laser Photonics Rev. **7**(6), 839–854 (2013).
13. N. Bhebhe, P. A. Williams, C. Rosales-Guzmán, V. Rodriguez-Fajardo, and A. Forbes, "A vector holographic optical trap," Sci. Rep. **8**(1), 17387 (2018).
14. M. P. Lavery, F. C. Speirits, S. M. Barnett, and M. J. Padgett, "Detection of a spinning object using light's orbital angular momentum," Science **341**(6145), 537–540 (2013).
15. V. D'ambrosio, N. Spagnolo, L. Del Re, S. Slussarenko, Y. Li, L. C. Kwek, L. Marrucci, S. P. Walborn, L. Aolita, and F. Sciarrino, "Photonic polarization gears for ultra-sensitive angular measurements," Nat. Commun. **4**(1), 2432 (2013).
16. F. Töppel, A. Aiello, C. Marquardt, E. Giacobino, and G. Leuchs, "Classical entanglement in polarization metrology," New J. Phys. **16**(7), 073019 (2014).
17. S. Berg-Johansen, F. Töppel, B. Stiller, P. Banzer, M. Ornigotti, E. Giacobino, G. Leuchs, A. Aiello, and C. Marquardt, "Classically entangled optical beams for high-speed kinematic sensing," Optica **2**(10), 864–868 (2015).
18. A. Belmonte, C. Rosales-Guzmán, and J. P. Torres, "Measurement of flow vorticity with helical beams of light," Optica **2**(11), 1002–1005 (2015).
19. X. Fang, H. Ren, and M. Gu, "Orbital angular momentum holography for high-security encryption," Nat. Photonics **14**(2), 102–108 (2020).
20. E. Otte, I. Nape, C. Rosales-Guzmán, C. Denz, A. Forbes, and B. Ndagano, "High-dimensional cryptography with spatial modes of light: tutorial," J. Opt. Soc. Am. B **37**(11), A309–A323 (2020).
21. X.-L. Wang, X.-D. Cai, Z.-E. Su, M.-C. Chen, D. Wu, L. Li, N.-L. Liu, C.-Y. Lu, and J.-W. Pan, "Quantum teleportation of multiple degrees of freedom of a single photon," Nature **518**(7540), 516–519 (2015).
22. J. Wang, J. Y. Yang, I. M. Fazal, N. Ahmed, Y. Yan, H. Huang, Y. Ren, Y. Yue, S. Dolinar, M. Tur, and A. E. Willner, "Terabit free-space data transmission employing orbital angular momentum multiplexing," Nat. Photonics **6**(7), 488–496 (2012).
23. N. Bozinovic, Y. Yue, Y. Ren, M. Tur, P. Kristensen, H. Huang, A. E. Willner, and S. Ramachandran, "Terabit-scale orbital angular momentum mode division multiplexing in fibers," Science **340**(6140), 1545–1548 (2013).
24. J. Liu, S.-M. Li, L. Zhu, A.-D. Wang, S. Chen, C. Klitis, C. Du, Q. Mo, M. Sorel, S.-Y. Yu, C. Xin-Lun, and J. Wang, "Direct fiber vector eigenmode multiplexing transmission seeded by integrated optical vortex emitters," Light: Sci. Appl. **7**(3), 17148 (2018).
25. A. E. Willner, "Vector-mode multiplexing brings an additional approach for capacity growth in optical fibers," Light: Sci. Appl. **7**(3), 18002 (2018).
26. T. Bauer, M. Neugebauer, G. Leuchs, and P. Banzer, "Optical polarization möbius strips and points of purely transverse spin density," Phys. Rev. Lett. **117**(1), 013601 (2016).
27. S. N. Khonina and I. Golub, "Ultrafast rotating dipole or propeller-shaped patterns: subwavelength shaping of a beam of light on a femtosecond time scale," Opt. Lett. **41**(7), 1605–1607 (2016).
28. V. Chille, S. Berg-Johansen, M. Semmler, P. Banzer, A. Aiello, G. Leuchs, and C. Marquardt, "Experimental generation of amplitude squeezed vector beams," Opt. Express **24**(11), 12385 (2016).
29. E. Pisanty, G. J. Machado, V. Vicu na-Hernández, A. Picón, A. Celi, J. P. Torres, and M. Lewenstein, "Knotting fractional-order knots with the polarization state of light," Nat. Photonics **13**(8), 569–574 (2019).
30. S. N. Khonina, A. P. Porfirev, and N. L. Kazanskiy, "Variable transformation of singular cylindrical vector beams using anisotropic crystals," Sci. Rep. **10**(1), 5590 (2020).
31. A. P. Porfirev, S. N. Khonina, and A. V. Ustinov, "Vector lissajous laser beams," Opt. Lett. **45**(15), 4112–4115 (2020).
32. S. Joshi, S. N. Khan, Manisha, P. Senthilkumaran, and B. Kanseri, "Coherence-induced polarization effects in vector vortex beams," Opt. Lett. **45**(17), 4815–4818 (2020).
33. N. Barré, M. Romanelli, M. Lebental, and M. Brunel, "Waves and rays in plano-concave laser cavities: I. geometric modes in the paraxial approximation," Eur. J. Phys. **38**(3), 034010 (2017).
34. Y. Shen, Z. Wan, Y. Meng, X. Fu, and M. Gong, "Polygonal vortex beams," IEEE Photonics J. **10**(4), 1–16 (2018).
35. Z. Wan, Z. Wang, X. Yang, Y. Shen, and X. Fu, "Digitally tailoring arbitrary structured light of generalized ray-wave duality," Opt. Express **28**(21), 31043–31056 (2020).
36. Y.-F. Chen, C. Jiang, Y.-P. Lan, and K.-F. Huang, "Wave representation of geometrical laser beam trajectories in a hemiconfocal cavity," Phys. Rev. A **69**(5), 053807 (2004).
37. Y.-F. Chen, J. Tung, P. Chiang, H. Liang, and K.-F. Huang, "Exploring the effect of fractional degeneracy and the emergence of ray-wave duality in solid-state lasers with off-axis pumping," Phys. Rev. A **88**(1), 013827 (2013).
38. J. Dingjan, M. van Exter, and J. Woerdman, "Geometric modes in a single-frequency Nd: YVO4 laser," Opt. Commun. **188**(5-6), 345–351 (2001).
39. Y. Shen, X. Yang, X. Fu, and M. Gong, "Periodic-trajectory-controlled, coherent-state-phase-switched, and wavelength-tunable SU(2) geometric modes in a frequency-degenerate resonator," Appl. Opt. **57**(32), 9543–9549 (2018).
40. Y. Shen, Z. Wang, X. Fu, D. Naidoo, and A. Forbes, "SU(2) Poincaré sphere: A generalized representation for multidimensional structured light," Phys. Rev. A **102**(3), 031501 (2020).
41. Y. Shen, X. Fu, and M. Gong, "Truncated triangular diffraction lattices and orbital-angular-momentum detection of vortex SU(2) geometric modes," Opt. Express **26**(20), 25545–25557 (2018).

Optics EXPRESS

42. J. Tung, H. Liang, T. Lu, K.-F. Huang, and Y.-F. Chen, "Exploring vortex structures in orbital-angular-momentum beams generated from planar geometric modes with a mode converter," Opt. Express **24**(20), 22796–22805 (2016).
43. J. Tung, T. Omatsu, H. Liang, K.-F. Huang, and Y.-F. Chen, "Exploring the self-mode locking and vortex structures of nonplanar elliptical modes in selectively end-pumped Nd: YVO_4 lasers: manifestation of large fractional orbital angular momentum," Opt. Express **25**(19), 22769–22779 (2017).
44. J. Pan, Y. Shen, Z. Wan, X. Fu, H. Zhang, and Q. Liu, "Index-tunable structured-light beams from a laser with an intracavity astigmatic mode converter," Phys. Rev. Appl. **14**(4), 044048 (2020).
45. P. Tuan, Y. Hsieh, Y. Lai, K.-F. Huang, and Y.-F. Chen, "Characterization and generation of high-power multi-axis vortex beams by using off-axis pumped degenerate cavities with external astigmatic mode converter," Opt. Express **26**(16), 20481–20491 (2018).
46. Y. Shen, X. Yang, D. Naidoo, X. Fu, and A. Forbes, "Structured ray-wave vector vortex beams in multiple degrees of freedom from a laser," Optica **7**(7), 820–831 (2020).
47. A. H. Dorrah, N. A. Rubin, A. Zaidi, M. Tamagnone, and F. Capasso, "Longitudinally variable polarization optics," in *2020 Conference on Lasers and Electro-Optics (CLEO)*, (2020), pp. 1–2.
48. Y. F. Chen, "Geometry of classical periodic orbits and quantum coherent states in coupled oscillators with SU(2) transformations," Phys. Rev. A **83**(3), 032124 (2011).
49. R. Blumel, *Advanced quantum mechanics: the classical-quantum connection* (Jones & Bartlett Publishers, 2011).
50. J. Babington, "Ray-wave duality in classical optics: crossing the feynman bridge," Opt. Lett. **43**(22), 5591–5594 (2018).
51. L. Allen, M. W. Beijersbergen, R. Spreeuw, and J. Woerdman, "Orbital angular momentum of light and the transformation of Laguerre-Gaussian laser modes," Phys. Rev. A **45**(11), 8185–8189 (1992).
52. M. W. Beijersbergen, L. Allen, H. Van der Veen, and J. Woerdman, "Astigmatic laser mode converters and transfer of orbital angular momentum," Opt. Commun. **96**(1-3), 123–132 (1993).
53. Y. Shen, Y. Meng, X. Fu, and M. Gong, "Wavelength-tunable Hermite-Gaussian modes and an orbital-angular-momentum-tunable vortex beam in a dual-off-axis pumped Yb: CALGO laser," Opt. Lett. **43**(2), 291–294 (2018).
54. J. Pan, Y. Shen, Z. Wan, X. Fu, H. Zhang, and Q. Liu, "Index-tunable structured-light beams from a laser with an intracavity astigmatic mode converter," Phys. Rev. Appl. **14**(4), 044048 (2020).
55. H. A. Nam, M. G. Cohen, and J. W. Noé, "A simple method for creating a robust optical vortex beam with a single cylinder lens," J. Opt. **13**(6), 064026 (2011).
56. H. Sridhar, M. G. Cohen, and J. W. Noé, "Creating optical vortex modes with a single cylinder lens," in *Complex Light and Optical Forces IV*, vol. 7613 (International Society for Optics and Photonics, 2010), p. 76130X.
57. Y.-F. Chen, C. Chang, C. Lee, J. Tung, H. Liang, and K.-F. Huang, "Characterizing the propagation evolution of wave patterns and vortex structures in astigmatic transformations of Hermite–Gaussian beams," Laser Phys. **28**(1), 015002 (2018).
58. S. N. Khonina, V. V. Kotlyar, V. A. Soifer, K. Jefimovs, P. Pääkkönen, and J. Turunen, "Astigmatic Bessel laser beams," J. Mod. Opt. **51**(5), 677–686 (2004).
59. V. V. Kotlyar, A. A. Kovalev, and A. P. Porfirev, "Astigmatic transforms of an optical vortex for measurement of its topological charge," Appl. Opt. **56**(14), 4095 (2017).
60. A. P. Porfirev and S. N. Khonina, "Astigmatic transformation of optical vortex beams with high-order cylindrical polarization," J. Opt. Soc. Am. B **36**(8), 2193 (2019).
61. V. Bužek and T. Quang, "Generalized coherent state for bosonic realization of SU(2) Lie algebra," J. Opt. Soc. Am. B **6**(12), 2447–2449 (1989).
62. Y. Chen, S. Li, Y. Hsieh, J. Tung, H. Liang, and K.-F. Huang, "Laser wave-packet representation to unify eigenmodes and geometric modes in spherical cavities," Opt. Lett. **44**(11), 2649–2652 (2019).
63. P.-H. Tuan, H.-C. Liang, K.-F. Huang, and Y.-F. Chen, "Realizing high-pulse-energy large-angular-momentum beams by astigmatic transformation of geometric modes in an Nd: YAG/Cr^{4+}: YAG laser," IEEE J. Sel. Top. Quantum Electron. **24**(5), 1–9 (2018).
64. M. A. Alonso and M. R. Dennis, "Ray-optical Poincaré sphere for structured Gaussian beams," Optica **4**(4), 476–486 (2017).